

International Journal of Modern Physics D
© World Scientific Publishing Company

Monte-Carlo Simulations of Thermal Comptonization Process in a Two Component Accretion Flow Around a Black Hole

Himadri Ghosh

*S.N. Bose National Centre for Basic Sciences,
JD-Block, Sector III, Salt Lake, Kolkata 700098, India.
himadri@bose.res.in*

Sandip K. Chakrabarti*

*S.N. Bose National Centre for Basic Sciences,
JD-Block, Sector III, Salt Lake, Kolkata 700098, India.
chakraba@bose.res.in*

Philippe Laurent

*IRFU, Service d'Astrophysique, Bat. 709 Orme des Merisiers, CEA Saclay, 91191
Gif-sur-Yvette Cedex, France, philippe.laurent@cea.fr*

Received Day Month Year

Revised Day Month Year

Communicated by Managing Editor

We compute the effects of thermal Comptonization of soft photons emitted from a Keplerian disk around a black hole by the post-shock region of a sub-Keplerian flow, known as the CENTrifugal pressure dominated BOUNDary Layer (CENBOL). We show that the spectral state transitions of black hole candidates could be explained either by varying the outer boundary of the CENBOL, which also happens to be the inner edge of the Keplerian disk, or by changing the central density of the CENBOL which is governed by the rate of the sub-Keplerian flow. We confirm the conclusions of the previous theoretical studies that the interplay between the intensity of the soft photons emitted by the Keplerian flow and the optical depth and electron temperature of the Comptonizing cloud is responsible for the state transitions in a black hole.

Keywords: accretion disk, black hole physics, shock waves, radiative processes, Monte-Carlo simulations

1. Introduction

For over quarter of a century, the Monte Carlo simulation has been found to be an essential tool to understand the formation of spectrum in compact bodies (Pozdnyakov, Sobol & Sunyaev, 1983). This followed the work of Sunyaev & Titarchuk (1980; hereafter ST80) which showed that the power-law component of a black hole

*Also at Indian Centre for Space Physics, Chalantika 43, Garia Station Rd., Kolkata 700084

spectrum is due to inverse Comptonization. More work (Sunyaev & Titarchuk, 1985; hereafter ST85) firmly established this. Hua & Titarchuk (1996) confirmed the conclusions drawn in Sunyaev & Titarchuk (1980, 1985) and Titarchuk (1994) using a Monte-Carlo simulation. Meanwhile, more efforts were given to understand the nature of the Compton cloud itself and generally it was believed that accretion disk coronas could be responsible for Comptonization.

In a deviation from the usual assumption that the corona of a disk (whose existence has been motivated only from solar science, and not through theoretical solutions) is indeed the Compton cloud, Chakrabarti & Titarchuk (1995, see, references therein; hereafter CT95) and Chakrabarti (1997, hereafter C97) pointed out that the post-shock region of a rotating sub-Keplerian flow could actually be the illusive Compton cloud and the Keplerian flow on the equatorial plane supplies soft photons to it to be inverse Comptonized. Simply put, in this so-called two component advective flow (TCAF) model, the state of a black hole is decided by the relative importance of the processing of the *intercepted* soft photons emitted from a Keplerian disk by the puffed-up post-shock region formed in the sub-Keplerian halo. This region exists primarily due to the centrifugal force which grows more rapidly than the gravitational force as the matter approaches the black hole. This is therefore termed as the CENtrifugal pressure supported BOundary Layer or simply CENBOL. If the CENBOL remains hot (generally due to smaller number of soft-photons from a Keplerian disk having lower accretion rate), and emits hard X-rays, it is the low/hard state since more power is in the hard X-ray region. On the contrary, if the CENBOL is cooled down by copious number of intercepted photons, the black hole goes back to the high/soft state. CT95 also pointed out that even in a high/soft state, some electrons should be energized by the momentum deposition due to the bulk motion of the electrons rushing towards the horizon. These photons would have a almost constant spectral slope. This was later verified by Monte-Carlo simulations (Laurent & Titarchuk 1999; 2001).

While the general results of ST80 & ST85 are of great importance, the computations in the literature were done with a few specific geometries of the cloud, such as plane slabs or spherical blobs. In reality, the geometry *must be* more complex, simply because of the angular momentum of matter (see, Chakrabarti, 1990 and references therein). Indeed, time dependent numerical simulations of sub-Keplerian flows (Molteni, Lanzafame & Chakrabarti, 1994; Molteni, Ryu & Chakrabarti, 1996) confirm the predictions in Chakrabarti (1990) and clearly show that the geometry of the flow close to a black hole, especially in the post-shock region, is more like a torus, very similar to a thick accretion disk conceived much earlier (e.g., Paczyński & Wiita, 1980; Rees et al. 1982 and references therein). In the latter case, the radial velocity was ignored but the angular momentum was assumed to be sub-Keplerian, while in the simulations of Molteni et al. (1994) the radial velocity was also included. In CT95 and C97, theoretical computation of the spectra was made by using the post-shock region as the Comptonizing cloud and by varying the accretion rates in

the Keplerian and sub-Keplerian components. Here too somewhat ideal geometry (cylindrical) was chosen so as to utilize the ST80 & ST85 results as far as the radiative transfer properties are concerned. A result with a real toroidal geometry can be handled only when the Monte-Carlo simulations are used.

In the present paper, we attempt to solve the problem of spectral properties using a thick accretion disk of toroidal geometry as the Compton cloud which is supposed to be produced by the sub-Keplerian inflow. The outer boundary of the thick accretion disk is treated as the inner edge of the Keplerian disk. One positive aspect in treating the CENBOL in this manner is that the distribution of electron density and temperature can be obtained totally analytically. In a more realistic case, one needs to solve the coupled transonic flow solution with radiative transfer. This would be very time consuming and is beyond the scope of the present work and will be reported elsewhere. The plan of our paper is the following. In the next Section, we discuss the geometry of the Compton cloud in our simulation. In §3, present the results of the simulations and in §4, we draw conclusions.

2. Geometry of the electron cloud and the soft photon source

In Fig. 1, we present a cartoon diagram of our simulation set up. In this paradigm picture (see, CT95 and references therein), the Compton cloud (CENBOL) is produced by the standing shock in the sub-Keplerian flow. CENBOL behaves like a boundary layer as it dissipates the thermal and bulk energy and produce hard X-rays and outflow/jets. The Keplerian disk is truncated and the inner edge is typically extended till the outer boundary of the CENBOL (shock location). However, in the soft states when the post-shock region is cooled down, the Keplerian disk can extend till the last stable circular orbit.

As the CENBOL is puffed up, its hot electrons intercept the soft photons and reprocess them via inverse Compton scattering. A photon originally emitted towards the CENBOL may undergo a single, multiple or no scattering with the hot electrons. The photons which enter the black holes are absorbed.

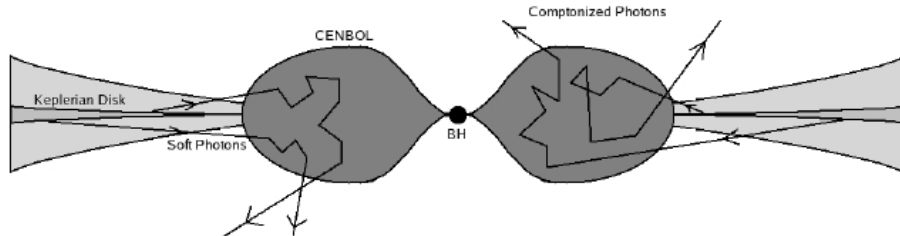


Fig. 1. A cartoon diagram of the geometry of the results of our Monte-Carlo Simulations presented in this paper. The puffed up post-shock region surrounds the black hole and it is surrounded by the Keplerian disk on the equatorial plane. A tenuous sub-Keplerian flow above and below the Keplerian disk is also present (CT95). Typical photon scattering paths are shown.

2.1. Distribution of temperature and density inside the Compton cloud

In order to verify that centrifugal pressure supported shocks found in Chakrabarti (1989) Molteni, Lanzafame and Chakrabarti (1994) carried out a two dimensional numerical simulation and found that this is indeed formed and the post-shock region (CENBOL) has all the properties of a thick accretion disk (Paczyński & Wiita, 1980). The simulation result is more realistic than a thick disk, since the flow also has a significant radial motion close to the horizon. For simplicity, in the present Monte-Carlo simulation, we assume the CENBOL to have the same analytical shape as an ideal thick disk (Fig. 2) and compute the matter density and temperature distribution using the prescription given in Chakrabarti, Jin and Arnett (1987) using the potential due to the black hole as:

$$\phi = \frac{\lambda^2}{2(r^2 - z^2)} - \frac{1}{2(r - 1)} \quad (1)$$

We have chosen the values of the parameters: $\beta = \frac{P_{gas}}{P} = 0.5$, polytropic index (n) = 3 and $\mu = 0.5$. The velocity, mass and distance scales are measured in units of c , the velocity of light, M_{bh} , the mass of the black hole and $r_g = 2GM_{bh}/c^2$, the Schwarzschild radius of the black hole. In this unit, the angular momentum of the disk is chosen to be $\lambda = 1.9$. The disk has a centre at 4 and the inner edge at 2.5. The number density of electrons within the CENBOL n is calculated from the matter density ρ , given by

$$\rho(r, z) = \left[\frac{\phi(r, z)}{n\gamma K} \right]^n \quad (2)$$

where the entropy constant K is given by,

$$K(\beta, \mu) = \left[\frac{3}{a} \frac{1 - \beta}{\beta^4} \frac{(k_b)^4}{(\mu m_p)^4} \right]^{\frac{1}{3}} \quad (3)$$

where a is the Stefan's radiation density constant, μ is the mean molecular weight, k_b is the Boltzmann constant and m_p is the mass of the proton. The temperature T_e of the electron cloud within CENBOL is given by

$$T_e(r, z) = \left[\frac{\beta \mu m_p}{k_b} K \right] \rho^{\frac{1}{3}} \quad (4)$$

In the simulation we have varied the outer edge (R_{out}) of the CENBOL to different values to change the size of the Compton cloud (Fig. 2). For simplicity, we carry out the simulations assuming an effective electron temperature T_{eff} and this was calculated using the prescription given in Sec. 2.4 of CT95.

2.2. Keplerian disk

The soft photons are produced from a Keplerian disk whose inner edge is at the outer edge (R_{out}) of the CENBOL, and the outer edge is at $500r_g$. The source of soft

photons have a multi-color blackbody spectrum coming from a standard (Shakura & Sunyaev, 1973) disk. We assume that the disk to be optically thick and the opacity due to free-free absorption is more important than the opacity due to scattering. The energy flux of the injected spectrum is given by:

$$F(r) = 5 \times 10^{26} (M_{bh})^{-2} \dot{M}_{17} (2r)^{-3} \left[1 - \sqrt{\frac{3}{r}} \right] \text{ergcm}^{-2} \text{sec}^{-1} \quad (5)$$

As the disk is optically thick, the emission is black body type with the local surface temperature:

$$T(r) = \left[\frac{F(r)}{\sigma} \right]^{1/4} \approx 5 \times 10^7 (M_{bh})^{-1/2} (\dot{M}_{17})^{1/4} (2r)^{-3/4} \left[1 - \sqrt{\frac{3}{r}} \right]^{1/4} K, \quad (6)$$

where, σ is the Stefan's radiation constant. The total number of photons emitted from the disk surface is obtained by integrating over all frequencies (ν) and is given by,

$$n_\gamma(r) = \left[16\pi \left(\frac{k_b}{hc} \right)^3 \times 1.202057 \right] (T(r))^3 \quad (7)$$

We divided the disk into different annuli each having an width of δr . The disk between radius r to $r + \delta r$ injects $dN(r)$ number of soft photons isotropically with black body temperature $T(r)$.

$$dN(r) = 2\pi r \delta r n_\gamma(r). \quad (8)$$

In the above equations, the mass of the black hole M_{bh} is measured in units of the mass of the Sun (M_\odot), the accretion rate \dot{M}_{17} is in units of 10^{17} gm/s. Unless otherwise stated, we chose $M_{bh} = 10$, accretion rate $\dot{m} = \frac{\dot{M}}{M_{edd}} = 1$ and $\delta r = 0.5r_g$. For the sake of completion of a simulation using a reasonable amount of computer time, we take a constant fraction of the number of photons (Eq. 9) from each annulus (see, Table 2 below). Because of the number of photons we select is way below the actual number, the absolute value of accretion rate itself is itself not very meaningful. However, the relative number of the intercepted photons and the number density of electrons inside CENBOL appears to be more important. The result also does not depend on the choice of δr as long as it is a fraction of a Schwarzschild radius. In Fig. 3, we show the distribution of the temperature (in keV) in the Keplerian disk and that in the CENBOL which we have used in our simulations. Different panels are for different values of the outer edge R_{out} (marked) of the CENBOL radius. We provide the effective temperature (T_{eff}) within the post-shock region in R_{out} in Table 1. These were obtained by changing the central density of the thick disk, which gave a temperature distribution inside CENBOL. Subsequently, CT95 was followed to obtain an effective temperature. In simulations, however, the actual temperature distribution was used.

2.3. Simulation Procedure

In a simulation, we randomly generated a photon out of the Keplerian disk and using another set of random numbers we obtained its injected direction. With another random number we obtained a target optical depth τ_c at which the scattering takes place. The photon is followed within CENBOL till the optical depth reached τ_c . At this point a scattering is allowed to take place and the energy exchange is computed through Compton or inverse Comptonization. The electrons are assumed to obey relativistic Maxwell's distribution inside CENBOL. The photon frequencies are also gravitationally red-shifted or blue shifted depending on its relative location change with respect to the black hole. The process is continued till the photon either leaves the CENBOL or is absorbed by the black hole.

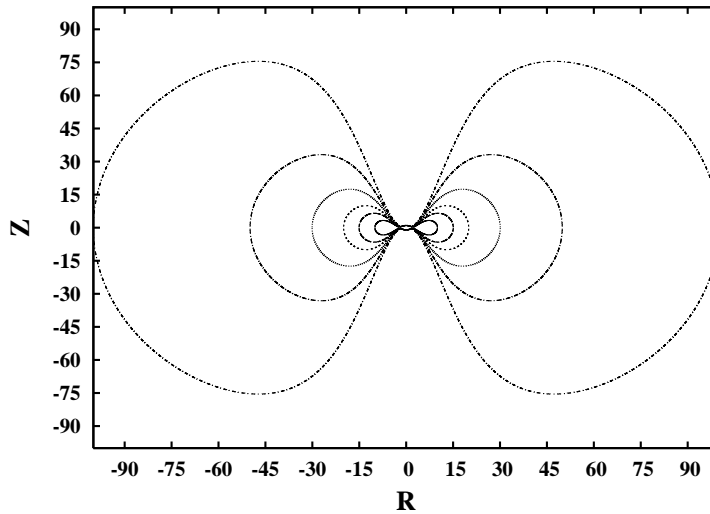


Fig. 2. Contours of constant temperature and density inside the CENBOL. Each of them has been used as the outer boundary in our simulations. $R_{out} = 10$ (solid line), 15 (large-dashed line), 20 (dashed line), 30 (dotted line), 50 (large dashed-dot line) and 100 (dashed-dot line).

3. Results and Discussions

In Table 2, we summarize all the cases for which the simulations have been presented in this paper. In Col. 1, various cases are marked. In Col. 2, the R_{out} and T_{eff} in keV are listed. In Cols. 3 and 4 we show the temperature (T_p) and the number of photons (dn_{in}) from the innermost annulus (R_{out}) of the Keplerian disk respectively. Columns 5, 6, 7 and 8 show the total number of injected photons (N_{inj}), number of the photons intercepted by the CENBOL (N_{int}), number of photons which suffered Compton scattering (N_{cs}) and the number of photons captured (N_{cap}) by the black hole respectively. In Column 9 we calculated the percentage p of the total injected

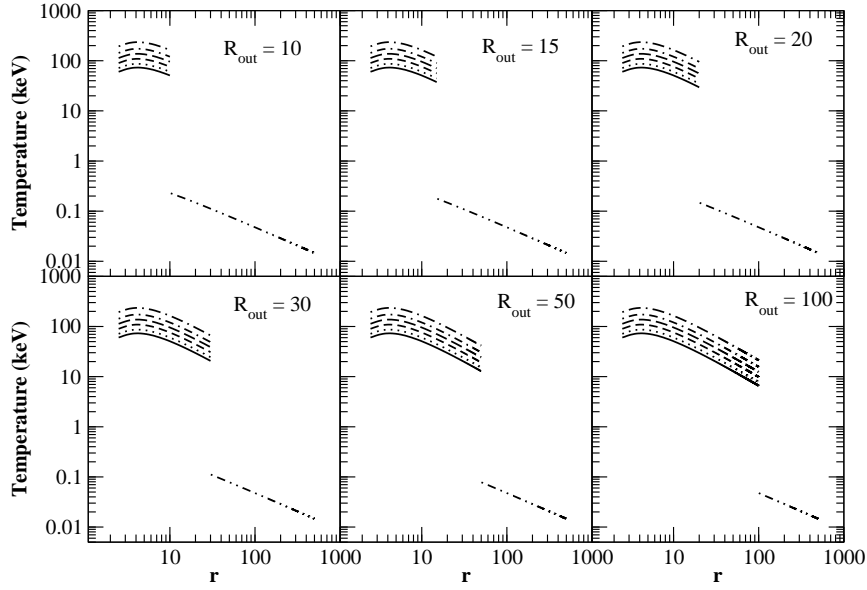


Fig. 3. Temperature distribution (in keV) inside the disk and the CENBOL region for different CENBOL outer boundary (R_{out}) and various central densities. Table 1 gives the relation between the central densities and the line styles.

Table 1
Central electron number densities (n in cm^{-3}) and the effective temperatures (in keV) for various outer edge R_{out} of the CENBOL used in this Paper

n (cm^{-3}) $\downarrow R_{out} \rightarrow$	10	15	20	30	50	100	Line style
7×10^{19}	61	54	50	46	43	42	Solid
1×10^{20}	73	64	59	54	51	50	Dotted
2×10^{20}	91	80	74	68	65	63	Short dashed
5×10^{20}	115	101	93	86	81	79	Big dashed
9×10^{20}	145	128	118	109	102	99	Dash-dotted
2×10^{21}	197	173	160	147	139	135	Big dash-dotted

photons that have suffered scattering through CENBOL. In Column 10, we present the energy spectral index α ($I(E) \sim E^{-\alpha}$) obtained from our simulations.

Table 2									
Case	R_{out}, T_{eff}	T_p	dn_{in}	N_{inj}	N_{int}	N_{cs}	N_{cap}	p	α
1a	10, 61	0.227	1633472	115150710	3042538	3024733	17805	2.627	2.10
1b	10, 73	-do-	-do-	-do-	3043059	3025416	17643	2.627	1.90
1c	10, 91	-do-	-do-	-do-	3041990	3024452	17538	2.627	1.65
1d	10, 115	-do-	-do-	-do-	3046115	3028743	17372	2.630	1.40
1e	10, 145	-do-	-do-	-do-	3043849	3026646	17203	2.628	1.15
1f	10, 197	-do-	-do-	-do-	3042031	3025183	16848	2.627	0.90
2a	15, 54	0.177	1139170	101283949	4011191	4005770	5421	3.955	1.12
2b	15, 64	-do-	-do-	-do-	4011473	4006227	5246	3.955	0.99
2c	15, 80	-do-	-do-	-do-	4012125	4007312	4813	3.957	0.82
2d	15, 101	-do-	-do-	-do-	4013872	4009153	4719	3.958	0.70
2e	15, 127	-do-	-do-	-do-	4007883	4003407	4476	3.953	0.57
2f	15, 173	-do-	-do-	-do-	4011584	4007483	4101	3.957	0.45
3a	20, 50	0.147	856814	91280716	4224551	4222011	2540	4.625	0.85
3b	20, 59	-do-	-do-	-do-	4222520	4219921	2599	4.623	0.75
3c	20, 74	-do-	-do-	-do-	4224950	4222666	2284	4.626	0.64
3d	20, 93	-do-	-do-	-do-	4221994	4219926	2068	4.623	0.54
3e	20, 118	-do-	-do-	-do-	4223468	4221663	1805	4.623	0.44
3f	20, 160	-do-	-do-	-do-	4222218	4220626	1592	4.623	0.34
4a	30, 46	0.111	558953	77355270	4369685	4368926	759	5.648	0.65
4b	30, 54	-do-	-do-	-do-	4366959	4366302	657	5.645	0.56
4c	30, 68	-do-	-do-	-do-	4367505	4366932	573	5.645	0.46
4d	30, 86	-do-	-do-	-do-	4371154	4370665	489	5.650	0.40
4e	30, 109	-do-	-do-	-do-	4368390	4367963	427	5.647	0.35
4f	30, 147	-do-	-do-	-do-	4372356	4372014	342	5.652	0.29
5a	50, 43	0.078	317226	60533079	4194919	4194781	138	6.930	0.56
5b	50, 51	-do-	-do-	-do-	4195709	4195582	127	6.931	0.50
5c	50, 65	-do-	-do-	-do-	4196096	4195988	108	6.931	0.44
5d	50, 81	-do-	-do-	-do-	4195788	4195715	73	6.931	0.38
5e	50, 102	-do-	-do-	-do-	4194298	4194244	54	6.929	0.32
5f	50, 139	-do-	-do-	-do-	4194327	4194282	45	6.929	0.28
6a	100, 42	0.048	142595	39539601	3780685	3780669	16	9.562	0.42
6b	100, 50	-do-	-do-	-do-	3801929	3801919	10	9.615	0.30
6c	100, 63	-do-	-do-	-do-	3808845	3808843	2	9.633	0.24
6d	100, 79	-do-	-do-	-do-	3812567	3812565	2	9.642	0.19
6e	100, 99	-do-	-do-	-do-	3814646	3814644	2	9.648	0.17
6f	100, 135	-do-	-do-	-do-	3815355	3815353	2	9.650	0.13

In Fig. 4, we summarize the results of all the cases, bunching them in groups with the same CENBOL size. Different cases are marked in each panel. Curves

(a) to (f) are from bottom to top respectively. Note that as T_{eff} is raised (a \rightarrow f), the spectrum becomes harder. Also, as R_{out} is increased, the percentage p of photons intercepted is also increased as the CENBOL becomes bigger. However, as the CENBOL size is increased, it becomes increasingly difficult to soften the spectrum with the same number of injected photons. Thus the spectrum becomes harder. This behaviour matches with the earlier theoretical predictions (Fig. 6 of C97). All the spectra are angle-averaged.

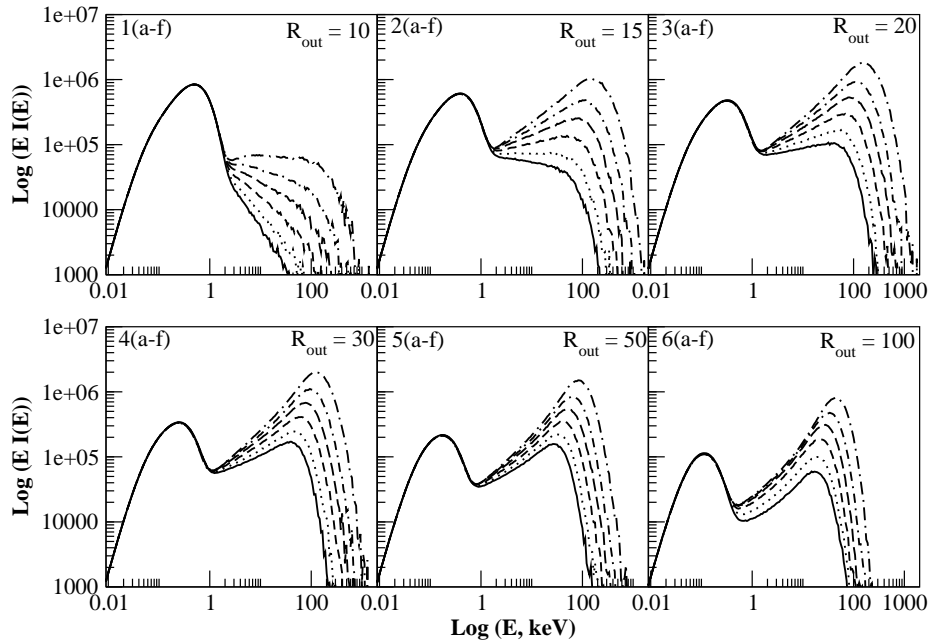


Fig. 4. Variation of the spectrum with increase of the effective temperature (T_{eff}) of the CENBOL for a fixed CENBOL size R_{out} . Each panel marks the cases for which the spectrum is drawn. Curves for (a) to (f) are from bottom to top respectively along the direction of increasing density and effective temperature.

In Fig. 5, we take one set, namely, Cases 3(a-f), for which $R_{out} = 20$ but the temperature distribution is varied which also changed T_{eff} . Here we draw each components, namely, the injected component (solid), the intercepted component (dotted) and the Comptonized component (dashed) separately. The net spectrum is shown as the dash-dotted curve. As we increase the temperature of the CENBOL, it becomes increasingly harder to cool the electrons, and thus the spectrum becomes

harder. In Fig. 6, we show two typical cases (Cases 3a and 3f) in which we wish to demonstrate how the power-law component has been produced. The solid curve represents the injected photons. The dotted, dashed, dotdashed and double dot-dashed curves show contributions from photons which underwent 1, 2, 3 and 4 or above number of scattering respectively. In Fig. 7, we plot the spectral variation with the CENBOL size. The cases correspond to Cases (1-6)a (Table 2) which are drawn in solid, dashed, small-dashed, dotted, long-dashed and small dash-dotted curves respectively. With the increase in size of the CENBOL, the spectrum becomes harder to cool, although the optical depth weighted effective temperature becomes lower. The latter causes the cut-off energy to become lower as well.

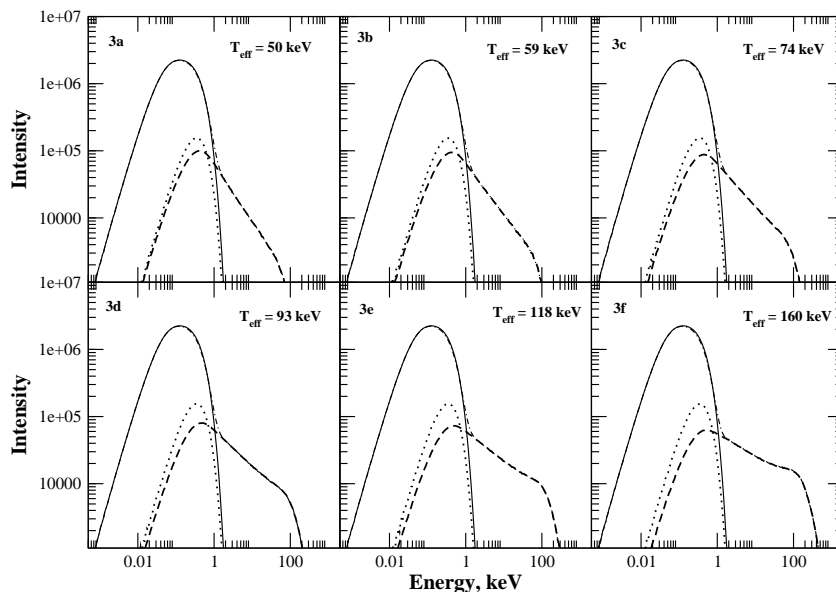


Fig. 5. Components of the emerging spectrum with a Keplerian disk outside $R_{out} = 20$ and their variation with the effective temperature of the CENBOL. As the electron temperature becomes hotter, the spectrum also gets harder.

In order to understand how the spectrum is influenced by the photons from different annuli, we compute the fraction of injected photons from each annulus which suffer scattering. In Fig. 8, we show the result for various CENBOL sizes. What we find is that when the CENBOL size is smaller, say, $R_{out} = 10$, only about 20% photons are intercepted from the nearest annulus, but the effect of the

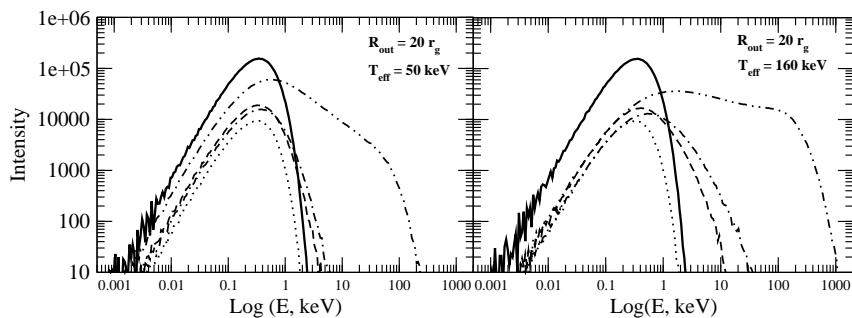


Fig. 6. Components of the emerging spectra with a Keplerian disk outside $R_{out} = 20$. The solid curve is for the injected photons. The dotted, dashed, dot-dashed and double dot-dashed curves show contributions from photons with number of scattering 1, 2, 3 and 4 or higher respectively. Cases 3a (left) and 3f (right) are shown.

annuli close to the periphery is negligible. On an average, however, only 2.6% get intercepted (see Table, 2). When the CENBOL size is bigger, say, $R_{out} = 100$, almost 50% of the photons from the annulus immediately outside the CENBOL gets intercepted and scattered. In this case, on an average, about 10% photons from the whole disk is scattered. From Table 2 we see that the nature of the above plot does not change for a particular CENBOL size even when the temperature is varied. So it is purely a geometric effect.

It is in general instructive to understand the behaviour when the black hole mass is much higher. In this case, the effective temperature could be much lower and the accretion rate will also be generally lower. In Table 3, we show the cases which were run for a massive black hole. We chose the mass to be $10^9 M_{\odot}$ and the accretion rate $\dot{m} = 0.001$. For the sake of comparison with the earlier cases, we selected the CENBOL parameters exactly same as in Cases 5(a-f). We note that for super-massive black hole, the Keplerian photons are cooler. Nevertheless, the inverse Comptonization extends the spectra to very high energies. This is because the source of the energy is the hot electron cloud itself. The variation of α , the

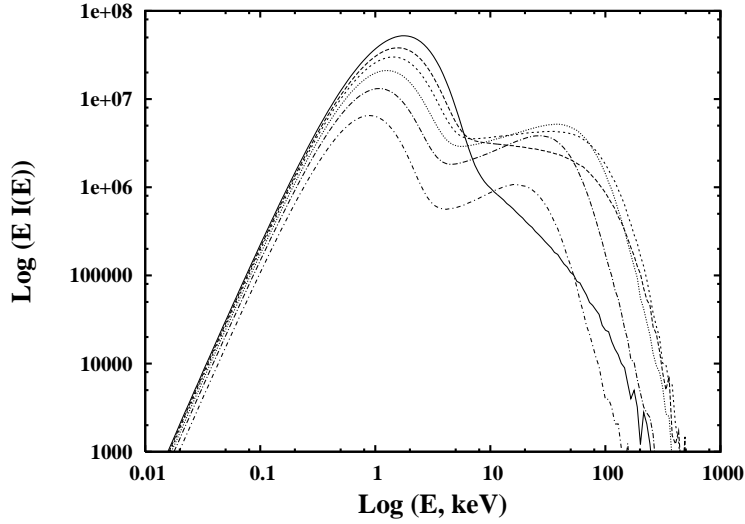


Fig. 7. Variation of the spectrum with the CENBOL size is shown. The cases correspond to Cases (1-6)a which are drawn in solid, dashed, small-dashed, dotted, long-dashed and small dash-dotted curves respectively. See Table 2 for parameters. With increase in size of the CENBOL the spectrum becomes harder to cool, although the optical depth weighted effective temperature becomes lower. The latter causes the cut-off energy to become lower.

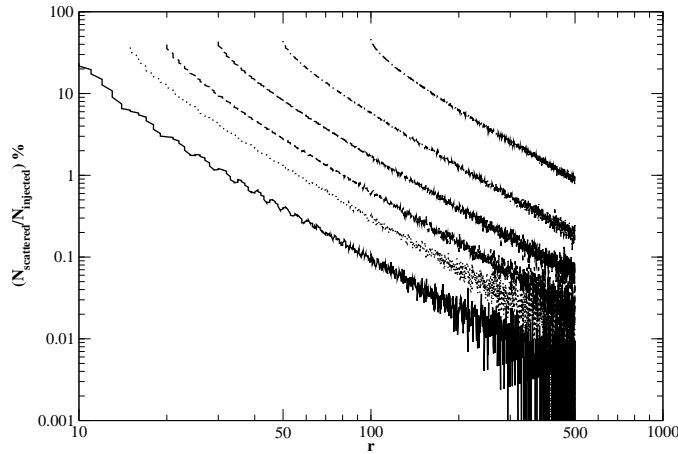


Fig. 8. Ratio of the scattered photons and the injected photons for different annuli of the Keplerian disk. Cases 1e to 6e are drawn from bottom to the top. The result is insensitive to the effective temperature of the electrons and generally depends on the relative geometry.

spectral index is given in the Table and they are marginally softer compared to what was observed for smaller black holes (Table 2).

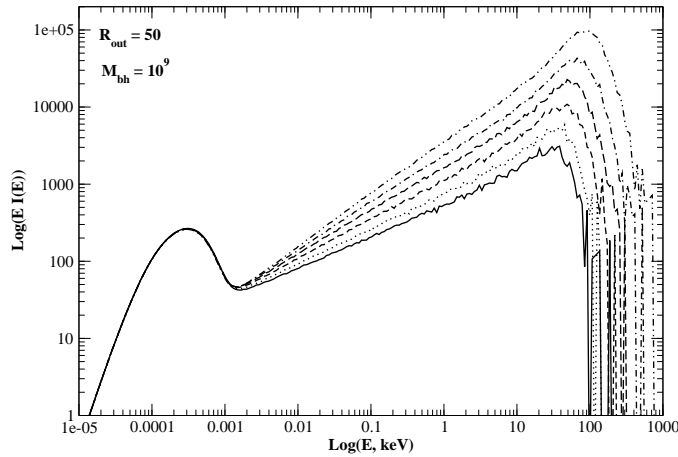


Fig. 9. Plot of $EI(E)$ for Cases 7(a-f) (presented in Table 3) are shown. For these simulations we considered $\dot{m} = 0.001$, $M_{bh} = 10^9 M_{\odot}$. Curves (a) to (f) are from bottom to top respectively.

Table 3

Case	R_{out}, T_{eff}	T_p	dn_{in}	N_{inj}	N_{int}	N_{cs}	N_{cap}	p	α
7a	50, 43	1.39×10^4	178412	34037468	2359549	2359463	86	6.932	0.59
7b	50, 51	-do-	-do-	-do-	2358802	2358725	78	6.930	0.55
7c	50, 65	-do-	-do-	-do-	2359201	2359145	57	6.931	0.50
7d	50, 81	-do-	-do-	-do-	2359354	2359313	41	6.931	0.44
7e	50, 102	-do-	-do-	-do-	2360152	2360114	38	6.934	0.39
7f	50, 139	-do-	-do-	-do-	2358340	2358314	26	6.929	0.32

4. Concluding remarks

In this paper, we have presented several results of Monte-Carlo simulation of Comptonization by hot electron clouds which surround the black hole in the form of a toroidal shaped centrifugal pressure dominated boundary layer. The soft photons are supplied by a Keplerian disk which reside just outside this cloud. Unlike previous Monte-Carlo methods where slab or spherical geometry have been considered, this is the first time that a realistic toroidal geometry has been chosen for the simulations.

We verify several of the previously reported conclusions obtained by theoretical methods. We find that for a given supply of the injected soft photons, the spectrum can become harder (i.e., spectral index α can go down) when either the optical depth is increased (electron number density goes up) and/or the electron temperature is increased. Furthermore, we found how the spectral shape changes when the Compton cloud expands and shrinks. We compute exactly what fraction of the photons are intercepted and processes and compute the percentage of scattered photons as functions of the flow variables. These results would be valuable to interpret the observational results from black hole candidates, especially when the spectral index is found to be changed.

In the present computation we assumed a stationary toroidal accretion disk. An inclusion of the radial component of velocity can produce an interesting effect, particularly visible when the spectral index is very high (in the so-called soft-state of the black hole). Here the electrons become so cold that the thermal Comptonization is ineffective and the power-law spectrum is dominated by the bulk motion Comptonization (CT95). This effect for spherical cloud has been demonstrated by Laurent & Titarchuk (1999) and can be considered to be a signature of a black hole candidate, since the radial velocity is high for infalling matter around such objects. In presence of rotational motion, preliminary results (Chakrabarti, Titarchuk, Kazanas & Ebisawa, 1996) show that the spectrum tends to become harder. Similarly, the outflow, which is generally believed to be formed out of the Compton cloud (here CENBOL) itself, can also Comptonize the injected photons and in certain situation could be very important. Simulations on these important cases. issues would be reported elsewhere.

Acknowledgments

The work of HG work is supported by a RESPOND project. He gratefully acknowledges the hospitality of Saclay, France where a part of this work was completed.

References

1. Chakrabarti, S.K., 1989, ApJ, 347, 365
2. Chakrabarti, S. K., 1990, Theory of Transonic Astrophysical Flows (World Scientific: Singapore).
3. Chakrabarti, S. K., 1997, ApJ 484, 313.
4. Chakrabarti, S. K., Jin, L., & Arnett, W. D., 1987, ApJ 313, 674.
5. Chakrabarti, S. K. & Mandal, S., 2006, ApJ 642, L49.
6. Chakrabarti, S. K. & Titarchuk, L. G., 1995, ApJ 455, 623.
7. Chakrabarti, S. K. & Titarchuk, L. G., Kazanas, D. & Ebisawa, K., 1996, A& A Supp. Ser., 120, 163.
8. Hua, J.M., & Titarchuk, L. G., 1996, ApJ 469, 280.
9. Laurent, P. & Titarchuk, L. G., 1999, ApJ 511, 289.
10. Laurent, P. & Titarchuk, L. G 2001, ApJ 562, 67.
11. Molteni, D., Lanzafame, G. & Chakrabarti, S.K., 1994, ApJ 425, 161.
12. Molteni, D., Ryu, D. & Chakrabarti, S.K., 1996, ApJ 470, 460.

13. Novikov, I. & Thorne, K. S., 1973, in: Black Holes, eds. C. DeWitt and B. DeWitt (Gordon and Breach, New York), 343.
14. Pozdnyakov, L.A., Sobol, I.M. & Sunyaev, R.A., 1983, *Astrophys. Sp. Sc. Reviews*, 2, 189.
15. Paczyński, B. and Wiita, P.J., 1980, *A&A*, 88, 23
16. Pozdnyakov, L. A., Sobol, J. M., & Sunyaev, R. A., 1983, *Space Sci. Rev.*, 2, 189.
17. Rees, M. J., Begelman, M. C., Blandford, R. D. & Phinney, E. S., 1982, *Nature*, 295, 17.
18. Rybicki, G. & Lightman, A. P., 1979, *Radiative Processes in Astrophysics* (New York: Wiley Interscience)
19. Shakura, N. I. & Sunyaev, R. A., 1973, *A & A*, 24, 337
20. Shapiro, S. L. & Teukolsky, S. A., 1983, *Black Holes, White Dwarfs and Neutron Stars - the Physics of Compact Objects* (John Wiley and Sons, New York).
21. Sunyaev, R.A. & Titarchuk, L.G., 1985, *A& A*, 143, 374
22. Sunyaev, R.A. & Titarchuk, L.G., 1980, *A& A*, 86, 121
23. Titarchuk, L., 1994, *ApJ* 434, 570